Available online at www.sciencedirect.com

SciVerse ScienceDirect

Physics Procedia 20 (2011) 149–159

Physics Procedia

Space, Propulsion & Energy Sciences International Forum - 2011

Recurrent Anholonomy in Curved Space Navigation Solved by the Riemann Zeta Function

B. Binder*

Quanics, P.O. Box 1247, 88679 Salem, Germany

Abstract

Navigation on curved surfaces has to handle additional nontrivial nonlinear geometric signals from (an)holonomy. Things may be even worse since propulsion recurrently couples back to the sensor signal. This effect can be experienced with orbiting gyroscopic sensors or spinning particles subject to spin-orbit coupling, which are just *G*-sensors of rotational acceleration. A solution to the rather simple orbital situation on spherically curved surfaces can be obtained by applying a Gudermannian mapping from precession patterns on the sphere onto holographic geometric phase patterns on the Poincaré disc by interference. This kind of stereographic mapping between surfaces of different constant curvatures induces the geometric extra rotations recurrently coupling back to the precession signal, where the fixed point solution to the emerging strange attractor is given by the functional equation of the Riemann zeta function.

PACS: 03.65.Vf , 04.20.Jb, 04.60.Pp, 04.62.+v, 05.45.-a, 98.10.+z
Keywords: Holonomy; Geometric Phase; Acceleration; Sensor; Riemann Zeta Function; Berry Phase; Sommerfeld Constant; Nonlinear; Field Equations; Spin; Precession; Gudermannian; Anholonomy

1. Introduction

Navigation in or on curved spaces is not trivial due to anholonomy effects of non-Euclidean geometry. In General Relativity (an)holonomy can be directly related to curvature with gyroscopic precession induced by curvature and/or torsion linearly related to the coupling strength. De Sitter was the first who predicted geodetic precession in curved space-time [1], where the gyroscope will be carried by parallel transport along the path of free fall [2]. If acceleration is superimposed to a strong gravitational field, where the spaceship navigational and propulsion control is managed by onboard acceleration

* Corresponding author. *E-mail address*: binder@quanics.com .

doi:10.1016/j.phpro.2011.08.014

sensors calibrated in flat space, it is not trivial to calculate the effective acceleration. The sensor vector signal is by the equivalence principle subject to two components: the gravitational field producing anholonomy and the acceleration due to propulsion controlled by the sensor. This situation could be reproduced in recent (later than 2008…) handhelds (race games) with *G*-control, where the radial accelerations are controlled by a *G*-sensor measuring the tilt of the handheld with respect to the gravitational field vector (vertical) and can be formulated as a theorem regarding acceleration sensors also used for acceleration control: *If a vector acceleration sensor calibrated in flat space is used to control the motion of a massive device (car, aircraft, ...) in curved spacetime, we get a nonlinear or even chaotic situation, since the propulsion initiated by the sensor recurrently affects anholonomy and the sensor vector signal controlling the acceleration.* Restricting the complexity to radial symmetry with orbital rotations and tilted sensors, the situation can be considerably simplified using Euler angles variables [3, 4]. Mapping the curved surface gyroscopic precession signal field to flat Poincaré space by a stereographic projection provides for the geometric phase patterns of extra rotations and provides for a simple strange attractor given by the sine/cosine map. In our example we will point to a solution given by the Riemann zeta function, which has a very prominent status in number theory and field theories. Since special precession or tilt angles of the attractor correspond to fixed points, bifurcations, and limit cycles we get a bifurcation dynamics especially for extreme curvature situations.

Nomenclature

α	coupling factor (unitless)	Θ	solid angle factor (unitless)
Γ	complex gamma function (unitless)	ζ	complex zeta function (unitless)
j	spin factor (unitless)	$\theta_\kappa, \varphi_\kappa, \psi$	gen. Euler angles (*rad*)
J	spin-charge factor (unitless)	$M, M_{\mathbb{N}}, M_0$	symmetry factor, monopole charge (unitless)
Ω	solid angle (*rad*)	x_0, x_1, x_2, q_1, q_2	Coordinates (*Meter*)
P	reflection factor (unitless)		
s	angular factor (unitless)		

2. Gyro-Sensors Dynamics With Euler Angles

We will describe the coupling of a gyro sensor by Euler's dynamical equations relating the three Euler angles to the three Euler frequencies and identify the coupling frequency shift that can be related to the geometric phase shift induced by anholonomy. In Euler's dynamical equations the angular velocity vector is expressed by three SO(3) Euler angles describing the motion of the advancing frame with respect to the inertial frame. With mass points rotating and precessing on the sphere (which is a classical connection) the three Euler angles shown in Figure 1. ϑ is the first Euler angle describing the precession *tilt* angle (the precession cone has half apex angle $\theta_\kappa = \pi/2 - \vartheta$), the second Euler angle φ describes the spin of the body rotor axis, the third Euler angle ψ is the *turn* of the axes. In Cartesian coordinates the rotor will precess around the z or x_0-axis. Assume that the rotor axis of a spherical rotating rotor precesses at frequency $\omega_\psi = d\psi/dt$. The temporal change of precession tilt called nutation is given by $\omega_\theta = d\theta/dt$, the rotator rotates at frequency $\omega_\varphi = d\varphi/dt$. The three frequency components of the axisymmetric advancing frame are given by Euler's gyroscope equations

$$\omega_0 = -\omega_\psi \sin\theta, \quad \omega_1 = \omega_\theta, \quad \omega_2 = \omega_\varphi + \omega_\psi \cos\theta. \tag{1}$$

The rotation around the z or x_0-axis experience a phase Δ and frequency shift $\omega_\Delta = d\Delta/dt$ due to anholonomy and/or external coupling with energy $E_{Coupling} = \frac{1}{2}\omega_\Delta{}^2$, which is part of the invariant From one Euler's equation, the other two follow by spherical symmetry. We consider parallel transport on a surface with constant curvature. The kinetic energy per mass T is given by

$$T = \tfrac{1}{2}(\omega_0{}^2 + \omega_1{}^2 + \omega_2{}^2) = \tfrac{1}{2}(\omega_\theta{}^2 + \omega_\psi{}^2 + \omega_\varphi{}^2) + \omega_\varphi(\omega_2 - \omega_\varphi)\,, \tag{2}$$

where the geometric precession phase shift from the frequency shift around the x_0 -axis well known as Berry-Hannay Phase [5] is one quantum extra rotation out of N in ω_2 denoted by

$$\omega_{\theta_{-\kappa}} = \frac{\mathrm{d}\varphi_{-\kappa}}{\mathrm{d}t} = \omega_0 - \omega_\psi = \frac{\omega_2}{N}\,. \tag{3}$$

With our strategy the quantum shift can be obtained by a stereographic projection given by the Gudermanns function $\theta_\kappa = Gd(\varphi_{-\kappa})$, mapping between spaces with different constant curvature κ (see Appendix B)

$$\frac{\mathrm{d}\theta_\kappa}{\mathrm{d}\varphi_{-\kappa}} = \cos\left(\sqrt{\kappa}\theta_\kappa\right) = \frac{1}{\cos\left(\sqrt{-\kappa}\varphi_{-\kappa}\right)} = \frac{1}{\cosh\left(\sqrt{\kappa}\varphi_{-\kappa}\right)} \text{ or } \sin\left(\sqrt{\kappa}\theta_\kappa\right) = \tanh\left(\sqrt{\kappa}\varphi_{-\kappa}\right), \tag{4}$$

with curvature-invariant Poincaré space distance $\kappa \leftrightarrow -\kappa$

$$q = \frac{\tan\left(\frac{1}{2}\sqrt{\kappa}\theta_\kappa\right)}{\sqrt{\kappa}} = \frac{\tan\left(\frac{1}{2}\sqrt{-\kappa}\varphi_{-\kappa}\right)}{\sqrt{-\kappa}} = \frac{\tanh\left(\frac{1}{2}\sqrt{\kappa}\varphi_{-\kappa}\right)}{\sqrt{\kappa}}\,. \tag{5}$$

Gudermanns function are stereographically mapping the precession θ_κ patterns on the sphere onto holographic geometric phase $\varphi_{-\kappa}$ patterns on the Poincaré disc by interference (see Appendix A and B, [6, 7]). We get with equation (4)

$$\omega_{\theta_{-\kappa}} = \omega_\psi\left[1 + \sin\left(\sqrt{\kappa}\theta_\kappa\right)\right] = \omega_\psi\left[1 + \tanh\left(\sqrt{\kappa}\varphi_{-\kappa}\right)\right] = \omega_\psi\,\frac{e^{\sqrt{\kappa}\varphi_{-\kappa}}}{\cosh\left(\sqrt{\kappa}\varphi_{-\kappa}\right)}, \tag{6}$$

and for a fixed frequency ratio ω_2 / ω_ψ a Coulomb/Kepler-Oscillator mapping relation [8, 9]

$$e^{-\sqrt{\kappa}\varphi_{-\kappa}} = N\frac{\omega_\psi}{\omega_2}\cos\left(\sqrt{\kappa}\theta_\kappa\right). \tag{7}$$

From the exponential function introduced by the Gudermannian the projection relating anholonomy to precession supports a sine or cosine map strange attractor in the precession angle

$$\frac{\mathrm{d}\theta_\kappa}{\mathrm{d}\varphi_{-\kappa}} = \cos\left(\sqrt{\kappa}\theta_\kappa\right) = -\frac{M}{j\pi}\sqrt{\kappa}\theta_\kappa \propto e^{-\sqrt{\kappa}\varphi_{-\kappa}} = e^{-\sqrt{\kappa}\theta_{-\kappa}\frac{M}{j\pi}},\ j\pi\varphi_{-\kappa} = \theta_{-\kappa}M\,, \tag{8}$$

where the integration constant follow from symmetry. If the projection onto the Poincaré disc shows a M-gonal symmetry corresponding to M invariant precession units or arms and monopole sources of geometric spin, where the 3rd dynamical invariant ω_2 is M-times the precession frequency providing for the frequency ratio $\omega_2 / \omega_\psi = M$, $\omega_{\varphi_{-\kappa}}$ contribute M geometric unit rotations $\Omega = \omega_{\theta_-}$ $(j = 1)$

$$\omega_2 = M\omega_\psi = \omega_\varphi + \omega_\psi\cos\theta\,,\ \frac{\Omega}{\omega_\psi} = \frac{\omega_{\theta_{-\kappa}}}{\omega_2} = N\,,\ \omega_{\theta_{-\kappa}} = M\Omega\,,\ \omega_{\theta_{-\kappa}} = j\Omega\,. \tag{9}$$

Assuming positive frequencies we get with equations (1)-(11) $\omega_2 > \omega_\varphi > \omega_\psi > \omega_{\varphi_{-\kappa}} > \omega_{\theta_{-\kappa}}$, where the minimum geometric shift is

$$\Omega = \omega_{\theta_{-\kappa}}(j=1) = \frac{\omega_2}{MN} = \frac{\omega_\varphi}{N(M-1)+j} = \frac{\omega_\psi}{N} = \frac{\omega_{\varphi_{-\kappa}}}{M} = \frac{\omega_{\theta_{-\kappa}}}{j\pi}. \tag{10}$$

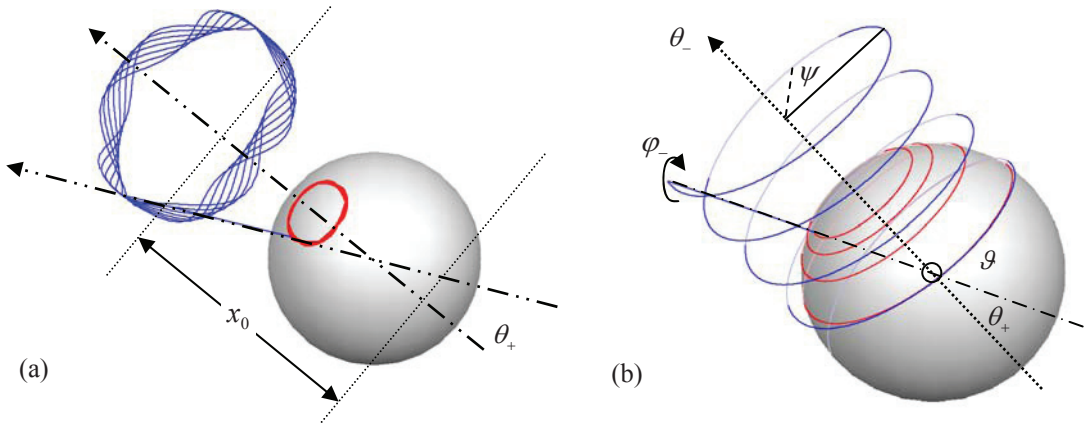

Figure 1: (a): Visualizing the Gudermannian projection for a special precession angle and distance. (b): The θ_+ loxodrome path on the sphere (red) mapped by a Gudermannian-Mercator to a helical path (blue) $M\theta_{-\kappa} = \pi j \varphi_{-\kappa} = \pi\varphi_0$ on the cylinder.

Gyroscopes are perfect acceleration sensors, where the spherical precession Euler angle θ_+ measures the acceleration. In this case we could identify some physical parameters given by a gyroscopic spin number j and spin-orbit coupling strength α_M. The coupling parameter α_M is responsible for the frequency shift and dynamical phase evolution within one precession loop according to

$$\alpha_M = \Omega \frac{\cos\theta_+}{\omega_{\varphi_-}} = \frac{\cos\theta_+}{M} = \frac{N-j}{NM}. \tag{11}$$

Equation (11) can characterize the fine structure of spin-orbit coupling [10, 11]. Since the rotator of the gyroscope (the acceleration sensor) is tilted by the precession angle θ_+ subject to the spherical curvature proportional to spin-orbit coupling strength α_M (de Sitter type) and charge spin-number j we get

$$\alpha_M = \frac{\theta}{j\pi} = \frac{\cos\theta_+}{M}. \tag{12}$$

This means the geometric phase component of the acceleration given by $1-\cos\theta_+$ will couple back to the sensor signal, see Figure 1a. If we fly on a loxodrome, we have constant anholonomy and straight lines in the Mercator projection corresponding to a helix on a cylinder, see Figure 1b. Thus, a Gudermann-Mercator stereographic projection of the spherical path can reveal the anholonomy effects, see Appendix A and B.

Equation (7) corresponds to the two Coulomb/Kepler-Oscillator mapping relations on the N-dimensional two sheeted hyperboloid ([8], equations 44, 55). Changing curvature we get the mapping relations on the N-dimensional spheres ([8], equation 17). In this paper they establish a relation between Coulomb and oscillator systems on N-dimensional spheres and hyperboloids for $N \geq 2$. They show that, as in Euclidean space, the quasiradial equation for the N+1 dimensional Coulomb problem coincides with the 2N-dimensional quasiradial oscillator equation on spheres and hyperboloids. Using the solution of the Schrödinger equation for the oscillator system, they construct the energy spectrum and wave functions

for the Coulomb problem. It has a long been known that the Coulomb and oscillator potentials are two paradigms in quantum mechanics that possesses dynamical or hidden symmetries: O(N+1) for motion in a Coulomb field and SU(N) for the oscillator. It is also known that the complete relation (not only for the radial part) is possible for only special dimensions (2,2), (3,4) and (5,8) respectively. The dual mappings in these cases are so-called Levi-Civita, Kustaanheimo-Stiefel and Hurwitz transformations. The oscillator potential ([8], equation 8) on the N-dimensional projection (see the Hamiltonian in Appendix B)

$$V_O(\varphi_{-\kappa}) \propto \kappa \tanh^2\left(\tfrac{1}{2}\sqrt{\kappa}\varphi_{-\kappa}\right) = \tan^2\left(\tfrac{1}{2}\sqrt{\kappa}\theta_\kappa\right) \propto \kappa \mathbf{q}^2 , \tag{13}$$

that appears in the kernel exponent of the neutral geometric phase interference pattern with Gaussian shape located in the overlap region between monopole patterns in the holographic projection [7], and is part of a Pöschl-Teller type equation and transformed to a corresponding N+1 dimensional Coulomb/Kepler potential term ([8], equation 15) by a Gudermann function

$$V_C(\theta_\kappa) \propto \frac{\kappa}{R} = \kappa \cot\left(\sqrt{\kappa}\theta_\kappa\right) = \frac{\kappa M \alpha_M}{\sqrt{\mathbf{x}^2}} . \tag{14}$$

3. Solution by the Zeta Functional Equation

To solve equation (12) we can take the reflection functional equation for the Riemann zeta function $\varsigma(s)$ with complex s and gamma function $\Gamma(1+s)$ [12, 13], see Figure 2

$$\cos\left(\tfrac{1}{2}\pi s\right)\frac{\Gamma(1+s)}{(2\pi)^s}\frac{\varsigma(s)}{\varsigma(1-s)} = \tfrac{1}{2}s . \tag{15}$$

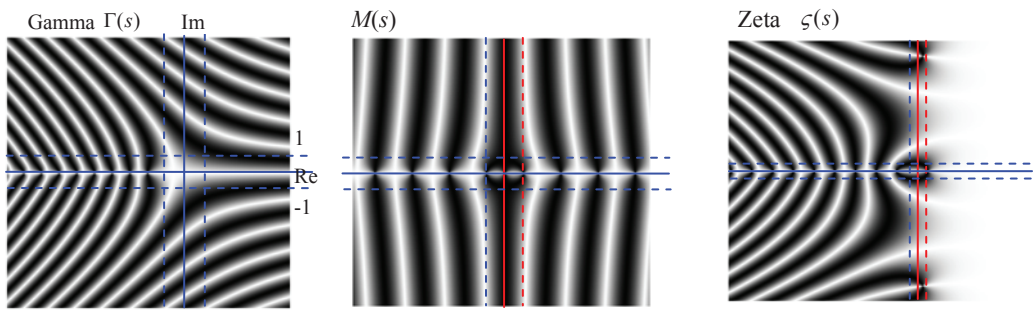

Figure 2: Left the gamma function, mid the MAP coupling function with critical strip $0 \le \mathrm{Re}\, s \le 1$ between red lines, right the zeta function with critical strip and first nontrivial zeros pair at the top and bottom.

Setting

$$\frac{M(s)}{j} = \frac{(2\pi)^s}{\Gamma(1+s)}\frac{\varsigma(1-s)}{\varsigma(s)}, \quad \tfrac{1}{2}s = j\alpha = \frac{\theta}{\pi} , \tag{16}$$

and fixing M to a specific value $M(s) \to M_0 \in \mathbb{R}$ we get with the functional equation (15) a solution to the cosine strange attractor of equation (12) that can be written as

$$\cos\left(j\pi\alpha\right) = M_0\alpha , \tag{17}$$

relating the real spin-orbit coupling constant α linearly to $\theta = j\pi\alpha = \frac{1}{2}\pi s$ and to the cosine function of θ. At fixed points or limit cycles the attractor in equation (17) attracts special amplitudes/angles. Visualizing complex analytic functions using Lundmark's domain colouring algorithm [14] in the complex plane reveals the functions landscapes, see Figure 2.

4. Monopole Gauss Flux

We can assign to the anholonomy acceleration sensor offset a monopole Gauss flux strength M characterizing the interaction of the gyroscope signal with the acceleration. Condition (12) corresponds geometrically to a conic rolling dynamics, a very common description of gyroscopic precession. A rolling translation connects the angular dynamics with the radial scale or amplitude of the oscillator for a given velocity. In Appendix C the Berry-Hannay geometric phase as a difference in the rolling dynamics of a rolling cone is visualized. $M(s) \to M_{\mathbb{N}} \in \mathbb{N}$ describes a resonant dynamics of the precessing gyroscope with rotation at M-gonal symmetry, which could be called quantum precession and Magic Angle Precession (MAP) [6, 10, 11]. With the solid angle $\Omega(1+s)$ subtended by the full surface of the unit sphere in $1+s$ dimensions we have from equation (16), see Figure 2

$$M_0 = \frac{j(s)}{\left(\frac{1}{2}\right)^s}\frac{\Omega(1+s)}{\pi}\frac{\varsigma(1-s)}{\varsigma(s)}, \quad \Omega(1+s) = \frac{\pi^{1+s}}{\Gamma(1+s)}. \tag{18}$$

Assuming that the monopole coupling emerges between $\varsigma(s)$ and its reflection $\varsigma(1-s)$ with a Gauss flux exchange through a surface with constant positive curvature in $1+s$ dimensions altering spin and charge, the monopole strength M_0 in equation (18) could be decomposed into a product of three terms:

- spin-charge factor $\mathrm{J}(s) = j(s)2^s$,
- solid angle factor $\Theta(s) = \Omega(1+s)/\pi$, and
- reflection factor $\mathrm{P}(s) = \varsigma(1-s)/\varsigma(s)$.

In terms of the above definitions, we have

$$M_0 = \mathrm{J}(s)\Theta(s)\mathrm{P}(s). \tag{19}$$

5. Strange Attractor and Chaotic Properties

For the chaotic situation there exists a possible physical model describing rotated rotations on curved surfaces, where the recursive chaotic equation $M_{\mathbb{N}}\theta_{i+1} = \pi j \cos\theta_i$ could describe a chaotic precession dynamics with precession angle $\theta_i = \frac{1}{2}\pi s_i$. $\Gamma(s)$, $M(s)$, and $\varsigma(s)$ are visualized in Figure 2. Iterating $s_i \to s_{i+1}(s_i)$ for a given quantized $M_{\mathbb{N}}$ and running j, the attractor can be written in terms of gamma and zeta functions

$$M_{\mathbb{N}} s_{i+1} = j\frac{(2\pi)^{s_i}}{\Gamma(s_i)}\frac{\varsigma(1-s_i)}{\varsigma(s_i)}. \tag{20}$$

The strange attractor in equation (20) can produce fractals and shows a Feigenbaum-type bifurcation spectrum, see Figure 3. Spin anomalies related to the magnetic moment are typical side effects of the holonomic effects induced by the Gauss spin flux through a surface with constant positive curvature in $1+s$ dimensions measurable as precession or wobbling.

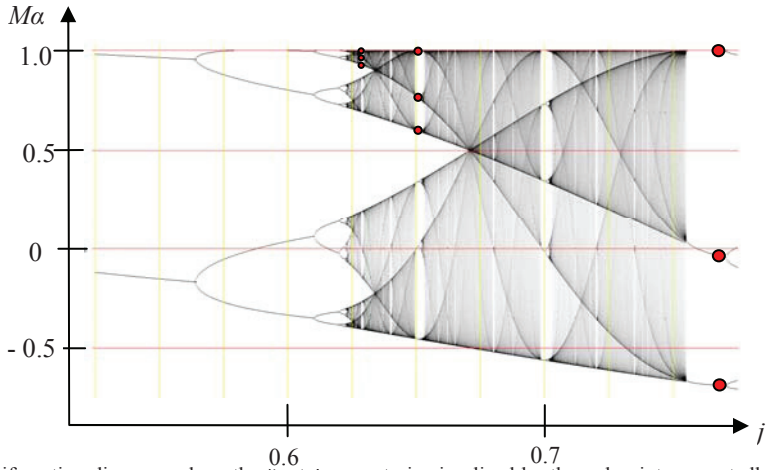

Figure 3: Fractal bifurcation diagram, where the fractal property is visualized by the red points, repeatedly emerging at different scales.

6. Summary and Conclusions

Taking Euler angular variables we have pointed to the situation, where a stereographic mapping between surfaces of different constant curvatures induces the geometric extra rotations recurrently coupling back to the precession signal. In this way the N+1-dimensional Coulomb/Kepler coupling can be mapped to a neutral oscillator on the N-dimensional two sheeted hyperboloids and spheres revealing the holographic nature of the coupling given by geometric phase patterns. The resulting transcendental relation (12) providing for magic tilt angles can be solved by the reflection functional equation for the Riemann zeta function, an extremely important special function of mathematics and physics that arises in definite integration and is intimately related with very deep results surrounding the prime number theorem [13]. To approach spin coupling anomalies we have assigned to the extra acceleration a monopole Gauss flux strength that could be decomposed into a product of three terms, a spin-charge factor $\mathrm{J}(s)$, a solid angle factor $\Theta(s)$, and a reflection factor $\mathrm{P}(s)$. This applies especially to orbiting gyroscopes or spinning particles, which are just G-sensors of rotational acceleration. Geometric phases play a central role in Maxwell-Coulomb interaction and quantum computation. Our model applies to generalized spin-orbit coupling constants probably relevant to the origin of the Sommerfeld fine structure constant [10]. It should be noted just for encouraging further research that the fixed point corresponding to the Dirac quantum condition for a real monopole charge number $M_{\mathbb{N}} = 137$ (and Cooper pair version with spin times charge $j = 1$) leads by iteration $s_i \to s_\infty = s$ in equation (20) to the fixed point with coupling strength $2s^{-1} = \alpha^{-1} = 137.036009...$, a generalized spin orbit coupling constant α that is within measurement accuracy (depending on the underlying theory and given assumptions) the value of the Sommerfeld fine structure constant. The resulting strange attractor in can produce fractals and shows a Feigenbaum-type bifurcation spectrum. Riemann's Zeta function appearing in general models for quantum chaos [16] with self-critical fractal power-law bifurcation density and auto-correlation spectrum fits well to recent developments [17]. Our model of recurrent anholonomy could be another basic example in this direction.

References

1. Misner, C., Thorne, K., Wheeler, J., *Gravitation*, Freeman, 1973.
2. Levi-Civita, T., Nozione di parallelismo in una varieta qualunque, Rend. Circ. Mat. Palermo (1917) **42**:173-205.

3. Osgood, W. F., On the Gyroscope, *Transactions of the American Mathematical Society* 1922 **23(3)**:240-264.
4. Osgood, W. F., *Mechanics*, MacMillan, New York, 1937.
5. Berry, M. V., Quantal phase factors accompanying adiabatic changes, Proc. *Roy. Soc. Lond. A* 1984 **392**:45.
6. Binder, B., Holonomy Attractor Connecting Spaces of Different Curvature Responsible for 'Anomalies' , in the proceedings of *Space, Propulsion & Energy Sciences International Forum* (SPESIF-09), edited by G. A. Robertson, AIP **CP1103**, Melville, New York, 2009 p. 629-655.
7. Binder, B., Nuclear and Crystal State Aspects of Overlapping Holographic Phase Patterns, in these proceedings of *Space, Propulsion & Energy Sciences International Forum (SPESIF-11)*, edited by Glen A. Robertson, Physics Procedia, Elsevier Science 2011.
8. Kalnins, E.G., Miller, W., Jr., Pogosyan, G.S., Coulomb-oscillator duality in spaces of constant curvature, *Journal of Mathematical Physics*, 2000 **41**:2629.
9. Kalnins, E. G., Miller Jr., W. and Pogosyan, G. S., *The Coulomb-oscillator* …, Phys. Atom. Nuclei 2002 **65**:1086-1094.
10. Binder, B., Berry's Phase and Fine Structure, PhilSci archive, 2002 (Preprint).
11. Binder, B. Magic Angle Chaotic Precession, in *Topics on Chaotic Systems: Selected Papers from CHAOS 2008 International Conference*, Singapore, World Scientific Books, 2008 p.31-42.
12. Riemann, B., *Über die Anzahl der Primzahlen unter einer gegebenen Größe*, Monatsberichte der Königlichen Preußischen Akademie der Wissenschaften zu Berlin, 1859 p. S.671–680.
13. Krantz, S. G., *Riemann's Zeta Function*. §13.2 Handbook of Complex Variables. Birkhäuser, Boston, 1999 p. 158-159.
14. Lundmark, H., Visualizing complex analytic functions using domain coloring, mai.liu.se, 2000.
15. Ballesteros, A. and Herranz, F. J., Maximal superintegrability of the generalized Kepler–Coulomb system on *N*-dimensional curved spaces, *J. Phys. A: Math. Theor.* 2009 **42**(24):245203.
16. Berry, M., Riemann's Zeta function: A model for quantum chaos? *Lecture Notes in Physics* 1986 **263**: 1-17.
17. Bogomolny, E., Riemann zeta function and quantum chaos, *Progress of theoretical physics supplement* 2007 **166**:19-44, (Preprint).

Appendix A: Stereographic Projection and Holography

The Gudermann functions and stereographic projection can be approached by Fresnel holographic considerations, see Figure 4.

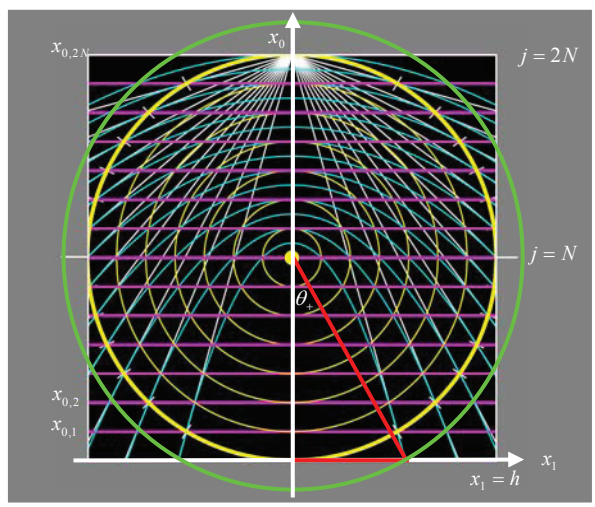

Figure 4. Stereographic projection (white lines), Fresnel interference paraboloids (cyan), plane wave (magenta) traveling in x_0 direction for $N = 7$, and the spherically diffracted wave (yellow and green).

The possible height coordinates of constructive interference at the j^{th} FZ with wave front travelling in x_0 -direction are given by

$$x_{0,j} = (j-1)\lambda \,, \tag{21}$$

where the green ring in Figure 4 corresponds to $j = 1$. The yellow ring shows the scattering height given by

$$x_{0,N} = h = N\lambda\,. \tag{22}$$

The spherically diffracted wave has a surface curvature κ that can be expressed by the number of waves N between diffraction and projection, see Figure 4, where the yellow point at the center is diffracting and the focusing point of the paraboloids and Fresnel zones. The radius of constructive interference at the observer image plane at $x_{0,j} = 0$ is the j^{th} FZ with

$$r_j = \left(1 + \frac{j}{N}\right)\lambda = h + \frac{j}{N}\lambda\,,\ r_j^2 = h^2 + \kappa\left(x_{1,j}^2 + x_{2,j}^2\right),\ \kappa = N^{-2}\,, \tag{23}$$

with Fresnel Zone ring radius in the image plane given by

$$s_j{}^2 = x_{1,j}{}^2 + x_{2,j}{}^2 = j\lambda\left(2N + j\right)\lambda = \left(2jN + j^2\right)\lambda^2\,. \tag{24}$$

The angle of interference is given by

$$\cos\theta_+ = \frac{N}{N+j} = \frac{h}{r_j}\,,\ \frac{j}{N}\lambda = r_j(1-\cos\theta_+)\,. \tag{25}$$

The Gudermannian function mapping the spherical angle θ_+ to the hyperbolic variable φ_- (and carrier of the geometric phase) is given by

$$\tan\left(\frac{\theta_+}{2}\right) = \tanh\left(\frac{\varphi_-}{2}\right) = \frac{\sqrt{\kappa}s_j}{(2+j/N)\lambda} = \frac{j\lambda}{s_j} = \frac{r_j - h}{\sqrt{r_j^2 - h^2}} = \sqrt{\frac{r_j - h}{r_j + h}} = \sqrt{\frac{j}{2N+j}}\,. \tag{26}$$

Appendix B: *N*-Dimensional Gudermannian Stereographic Projection

Consider spaces of constant curvature $\kappa \in \mathbb{R}$ representing for $\kappa \in \{1, 0, -1\}$ {spherical, flat, hyperbolic} surfaces in ambient Weierstrass coordinates [15] with

$$x_0{}^2 + \kappa\mathbf{x}^2 = r^2\,,\ (x_0, \mathbf{x}) = (x_0, x_1, ..., x_N) \subset \mathbb{R}^{N+1}\,, \tag{27}$$

With curvature $|\kappa| > 0$ dimensionality can be reduced by a N-dimensional stereographic projection to Poincaré space coordinates $\mathbf{q} = (q_1, ..., q_N) \in \mathbb{R}^N$ without (holographic) depth x_0

$$x_0{}^2 + \kappa\mathbf{x}^2 \longrightarrow \mathbf{q}^2\,,\ \mathbf{q} = (q_1, ..., q_N) \in \mathbb{R}^N \tag{28}$$

related by

$$\mathbf{x} = r\frac{2\sqrt{\kappa}\mathbf{q}}{1+\kappa\mathbf{q}^2}\,,\ \frac{x_0}{r} = \frac{\mathrm{d}\,\theta_\kappa}{\mathrm{d}\,\varphi_{-\kappa}} = \cos\left(\sqrt{\kappa}\theta_\kappa\right) = \frac{1-\kappa\mathbf{q}^2}{1+\kappa\mathbf{q}^2}\,,\ ds^2 = \kappa\mathrm{d}\theta_\kappa{}^2 = \frac{4\mathrm{d}\mathbf{q}^2}{\left(1+\kappa\mathbf{q}^2\right)^2} \tag{29}$$

and Gudermann curvature-invariant $\kappa \leftrightarrow -\kappa$ radial distance on the Poincaré disc according to equation (4) and (26)

$$\sqrt{\mathbf{q}^2} = |\mathbf{q}| = q = \tan\left(\tfrac{1}{2}\sqrt{\kappa}\theta_\kappa\right) = \pm\frac{1}{\sqrt{\kappa}}\sqrt{\frac{1-\cos\left(\sqrt{\kappa}\theta_\kappa\right)}{1+\cos\left(\sqrt{\kappa}\theta_\kappa\right)}}\,. \tag{30}$$

The image of the stereographic projection is determined by a scalar $\lambda_\kappa > 0$ that is related to the holographic depth x_0 and to a radial distance R_κ (ratio) on the image surface [15]

$$R_\kappa = \frac{\sqrt{\mathbf{x}^2}}{x_0} = \frac{2\sqrt{\mathbf{q}^2}}{1-\kappa\mathbf{q}^2} = \tan\left(\sqrt{\kappa}\theta_\kappa\right). \tag{31}$$

With these coordinates and curvature-invariant notation we can not only describe a holographic system, but also describe a maximally super-integrable geodesic flow between spaces with constant curvature κ providing for Kepler/Coulomb, oscillator, monopole, Pöschl-Teller, and centrifugal potentials in the *N*-dimensional Hamiltonian [15] given by

$$H = \frac{\mathbf{q}^2}{2R_\kappa{}^2}\left\{\mathbf{p}^2 + \frac{\mu^2}{\mathbf{q}^2} + \sum_{i=1}^{N}\frac{b_i}{q_i^2}\right\} + \frac{1}{R_\kappa}, \tag{32}$$

where the sum are centrifugal contributions and the kinetic energy is given by

$$T = \frac{\mathbf{q}^2\mathbf{p}^2}{2R_\kappa{}^2} = \frac{\mathbf{p}^2}{2\lambda_\kappa{}^2}, \ \mathbf{p} = \lambda_\kappa{}^2\dot{\mathbf{q}}, \ \dot{\mathbf{q}} \propto \omega. \tag{33}$$

Appendix C: The Geometry Behind $M\theta_+ = \pi j\cos\theta_+$

The classical geometry (Figure 5) for a positive curvature involves a stereographic Gudermann/Mercator projection with holographic properties (Appendix A) and a geometric phase (Berry) $\gamma_{Berry} = 2\pi(1-\cos\theta_+) = 2\pi/N$ due to the mapping of spin on a curved surface (precession) onto a flat surface (Appendix B). The classical physics geometry can serve as a basic model of spin-orbit interaction. One could consider a cone rolling on a plane, where the diameter of the circular rolling path is M times the diameter of the rolling contact circle with cone apex $2\vartheta = \pi - 2\theta_+$ and wobbling or precession angle θ_+ (Binder, 2002). In quantum physics this geometry corresponds to the mapping of a neutral oscillator potential stereographically to a Coulomb/Kepler potential, where M is the Dirac quantized monopole charge with integral $M = M_{\mathbb{N}} \in \mathbb{N}$ (source of geodesic spin flux). A modification is given by a spin quantum number j changing the number of spin/winding/cone rotations and the Berry phase for one period according to $M \to M/j$ and $\gamma_{Berry} \to j\gamma_{Berry}$.

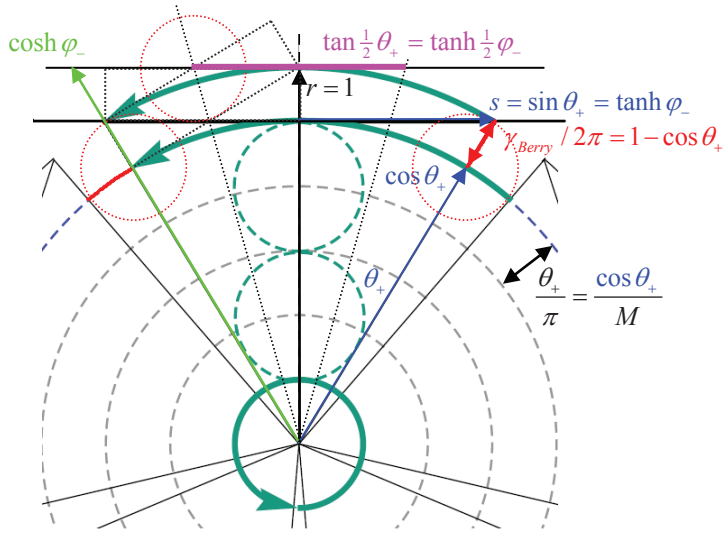

Figure 5. The geometric phase γ_{Berry} is the radius of the dashed red rings, here $M = 5$. The dark green arc lengths are all $2\theta_+$, θ_+ is the Gudermann function of φ_-.